

Equilibrium Geometries and Associated Energetic Properties of Mixed Metal–Silicon Clusters from Global Optimization

Jianhua Wu and Frank Hagelberg*

Computational Center for Molecular Structure and Interactions, Department of Physics,
Atmospheric Sciences, and General Science, Jackson State University, Jackson, Mississippi 39217

Received: December 16, 2005; In Final Form: March 9, 2006

The structural properties of the cluster series $\text{Me}_m\text{Si}_{7-m}$ ($\text{Me} = \text{Cu}$ and Li , $m \leq 6$) are studied by density functional theory (DFT) employing a plane wave basis. The equilibrium geometries and energetic properties of these clusters are obtained by use of the simulated annealing procedure in conjunction with the Nosé thermostat algorithm. The lowest energy isomer thus obtained is analyzed by density functional theory at the B3LYP/6-311+G(d,p) level including all electrons. Pentagonal ground state structures derived from the D_{5h} equilibrium geometries of both Si_7 and Cu_7 are obtained for $\text{Cu}_m\text{Si}_{7-m}$ with $m < 6$. The $\text{Li}_m\text{Si}_{7-m}$ clusters, in contrast, tend toward adsorption geometries where m Li atoms are attached to a Si_{7-m} framework with pronounced negative charge. For both $\text{Li}_m\text{Si}_{7-m}$ and $\text{Cu}_m\text{Si}_{7-m}$, a marked decrease of the energy gap is found as the number of metal atom constituents increases.

Introduction

Atomic clusters containing no more than a few hundred particles have been shown to display pronounced size-dependent properties,¹ such as geometric and electronic structure, binding energy, and melting temperature. A large and rapidly growing range of applications has been identified for nanoclusters. Thus, in view of their very favorable surface/volume ratio, these species have been utilized as catalysts.² More recently, much attention has been paid to the use of nanoclusters in a biological context. For example, gold nanoparticles studded with short segments of DNA³ could form the basis of an easy-to-read procedure for identifying genetic sequences.⁴

Substantial efforts of both theorists and experimentalists have focused on elucidating the geometric, electronic, and energetic features of pure silicon clusters.^{5–15} These studies were motivated chiefly by the fundamental interest in the size evolution of silicon from the scale of several atoms to the crystalline phase as well as the prospect of applications in the field of electronic materials. Photodissociation⁵ and collision-induced dissociation experiments have shown that both Si_6 and Si_{10} have exceptional stability, consistent with their “magic” behavior as observed in the mass spectra of Si clusters.⁶

The electronic structure of small metal clusters has long been a subject of intensive theoretical and experimental studies, because of its importance for the understanding of metal–metal interactions and its relevance for catalysis and photography. Alkali metal clusters, such as sodium and lithium clusters,^{16–20} have received the most attention, which is related to the simplicity of these systems, with each metal atom contributing only one valence electron. Further, detailed investigations have been devoted to transition-metal clusters, and among them prominently noble metal clusters.^{21–23}

At low temperatures, the most favored structure of a cluster of N particles is the one that minimizes its total energy. Within the Born–Oppenheimer approximation, the preferred geometry is given by the global minimum of the total cluster geometry as a

function of the coordinates of the atomic cores, defining the potential-energy surface (PES). In the case of Li clusters (Li_N), systematic ab initio configuration–interaction studies for $N \leq 9$ have shown that the lowest isomers are planar up to the pentamer.¹⁸ At $N = 6$, Ishikawa et al.¹⁹ reported a three-dimensional D_{4h} structure with slightly lower energy than the planar triangle and the pentagonal pyramid.

The energetics of small copper clusters has been extensively treated in a recent review by Alonso.²¹ Several ab initio calculations²¹ have been performed for $N \leq 10$, again comparing a set of plausible structures. There is evidence of planar equilibrium shapes up to an $N = 5$ or $N = 6$ maximum, as suggested by recent density functional theory (DFT) calculations.²² For $N = 13$, DFT computations indicate a preference of the icosahedron over the cuboctahedron.²³

The structures of Si_n ($n = 4–13$) clusters have been studied extensively by both ab initio and density functional approaches. For a review, the reader is referred to ref 11. The ground state of Si_4 is a planar rhombus (D_{2h}) in the neutral and anionic states. The ground state of Si_5 is a compressed trigonal bipyramid (D_{3h}), while Si_6 and Si_7 adopt the structures of a C_{2v} edge-capped trigonal bipyramid and a D_{5h} pentagonal bipyramid, respectively. The latter geometry has also been identified as the equilibrium structure of the metal clusters Li_7 ¹⁸ and Cu_7 .²²

Metal-doped silicon clusters exhibit a richer variety of geometric arrangements than pure silicon clusters. The metal atom in the Si_n cluster stabilizes the pure Si cluster. Beck²⁴ used a laser vaporization supersonic expansion technique to investigate MeSi_n ($\text{Me} = \text{Cu}$, Cr , Mo , and W) clusters by means of mass spectrometry and reported that they turned out to be more stable toward photofragmentation than bare Si_n clusters of similar size. Employing an ion trap method, Hiura et al.²⁵ produced metal atom encapsulating Si cluster ions of composition MeSi_n^+ ($\text{Me} = \text{Hf}$, Ta , W , Re , Ir , etc., with $n = 9, 11, 12, 13, 14$). Further analysis revealed that Si_n clusters with endohedral metal atom impurities are characterized by enhanced stability, strong size selectivity, and a large energy gap between the highest occupied molecular orbital (HOMO) and the lowest

* Corresponding author.

unoccupied molecular orbital (LUMO). The respective experimental findings stimulated several computational projects on the geometric, electronic, and energetic properties of metal-doped silicon clusters.^{12,26–30}

Mixed clusters combined of both types of constituents, metal and semiconductor components, have been shown to occur with stoichiometries typical for the metal–semiconductor interface.^{31,32} These hybrids are of substantial impact on the properties of the interface as well as the semiconductor. Clusters of the form Cu_xSi_y , containing multiple copper atoms, were detected in experiment.^{31,32} To our knowledge, no theoretical investigation on these species has been presented so far. In this contribution, we study the geometric and energetic features of $\text{Me}_m\text{Si}_{7-m}$ ($\text{Me} = \text{Cu}$ and Li , $m \leq 6$) clusters. The choice of these systems is motivated by the similarity of the pure Si_7 , Li_7 , and Cu_7 clusters which all stabilize in D_{5h} symmetry, thus imposing “symmetry boundary conditions” on $\text{Me}_m\text{Si}_{7-m}$ ($\text{Me} = \text{Cu}$ and Li , $m = 1, 2, \dots, 6$). On the other hand, Li and Cu , representing the alkali group (IA) and the noble metal group (IB) of the periodic system, are expected to display strongly differing behavior when integrated into a Si_n cluster. Thus, the most loosely bound electron of Li is easily transferred to the Si constituents. In Li_mSi_n clusters, therefore, Li atoms will act as electron donors and Si atoms as the receptors. Cu atoms, however, have been shown to form covalent bonds with Si atoms^{12,33} and, correspondingly, to adopt substitutional positions in Si_n clusters.³⁴ How does this fundamental difference impact the geometries, stabilities, and bonding features of the mixed species $\text{Me}_m\text{Si}_{7-m}$ with $\text{Me} = \text{Li}, \text{Cu}$?

To eliminate the dependence on the initial geometry, and to reduce the probability for trapping the system in a higher minimum than the lowest minimum of the potential-energy surface, a global optimization scheme has to be applied as opposed to a local relaxation method. The need for a global procedure is strongly intensified in the present case where species consisting of mixed constituents are considered, since the set of candidate structures is increased by the number of possible permutations of the two differing elements. The simulated annealing approach⁷ has been demonstrated to be successful in identifying global minima, although it met with some difficulties for large clusters.

In this work, we employ *ab initio* molecular dynamics on the basis of the simulated annealing method^{35,36} to investigate species of the form $\text{Me}_m\text{Si}_{7-m}$ ($\text{Me} = \text{Cu}$ and Li , $m \leq 6$). To confirm the lowest energy isomers, we have also applied various quantum chemical methods including density functional theory (DFT) at the B3LYP/6-311+G(d,p) level, taking all electrons into account.

In the following, we outline the computational method; subsequently, the calculated results are presented and discussed. Finally, we add some concluding remarks.

Theoretical Approach

Global geometry optimizations have been performed using the density functional theory (DFT) based Vienna *ab initio* simulation package (VASP).^{35,36} More specifically, the finite temperature version of local density functional (LDF) theory, as developed by Mermin,³⁷ is utilized in conjunction with the exchange–correlation functional given by Ceperley and Alder and parametrized by Perdew and Zunger.³⁸ It has been shown that the Hellmann–Feynman scheme yields a valid description of the forces within the DFT formalism also at finite temperature. Instead of Fermi–Dirac broadening of the one-electron energies, it may be computationally convenient to choose

Gaussian broadening which is used in this contribution. The width of the Gaussian distribution was selected as 0.01 eV; the total energy of the system refers to the limit of vanishing width.

The generalized Kohn–Sham equations³⁹ are solved employing a residual minimization scheme, namely, the direct inversion in the iterative subspace (RMM-DIIS) method.^{40,41} The interaction between valence electrons and core ions is described by the projector-augmented wave (PAW) method⁴² applying a generalized gradient correction (GGA), where the exchange–correlation functional of Perdew and Wang⁴³ (PW91) was used. In the case of Li atoms, all electrons (1s and 2s shells) are treated as valence electrons; the energy cutoff for the plane wave basis set is chosen as $E_{\text{cut}} = 272$ eV, while that for the augmentation charges is $E_{\text{aug}} = 428$ eV. For Cu atoms, 3d and 4s electrons are included in the valence system; the values for the energy cutoff are $E_{\text{cut}} = 273$ eV and $E_{\text{aug}} = 516$ eV, respectively. For Si atoms, the valence system comprises the 3s and 3p shells, and E_{cut} and E_{aug} are set at 245 and 322 eV, respectively.

To examine the reliability of the exchange–correlation functional on which the results of our manuscript are based, we carried out computations using the Perdew–Burke–Ernzerhoff (PBE) functional⁴⁴ for the cluster CuSi_6 as a test case. The optimizations performed with these two potentials yield the same type of equilibrium geometry, that is, a substitutional structure based on the pentagonal shape of Si_7 . The bond lengths obtained in the two cases deviate by about 2%.

The atomic motion is described using Nosé dynamics,⁴⁵ generating a canonical ensemble. The Nosé thermostat corresponds to a method for simulating a canonical ensemble at a selected temperature. The fictitious thermostat mass (Q), which determines the response of the heat bath to fluctuations of the ionic system, must be sufficiently small to allow the system to approach equilibrium fast enough and sufficiently large to yield correct values for the energy fluctuations of the ionic system.⁴⁶ In each individual case considered in the present work, we adjusted Q such that the period of the thermostat is equal to about 120 time steps.³⁵

The ionic equations of motion are integrated using a fourth-order predictor–corrector algorithm^{35,47,48} which allows the use of time steps as large as $t = 3.0$ fs with good energy conservation.

In our simulation, the initial configuration was realized by a random distribution of atoms with 2.6 Å as the lower limit of the distance between any atom pair. Periodic boundary conditions were imposed on a cubic cell with of dimension $16 \text{ \AA} \times 16 \text{ \AA} \times 16 \text{ \AA}$. By analyzing the atomic trajectories as they evolve during the simulation, we find that the minimal distance between atoms in neighboring supercells is larger than 9 Å, making the interaction between supercells negligible. Each simulation started at a temperature of $T = 2000$ K and was extended at this temperature over a period of 9.0 ps (3000 time steps), allowing the system to attain equilibrium. Subsequently, the hot clusters were cooled slowly and uniformly to zero temperature during a time interval of 30.0 ps (10 000 time steps). Finally, the geometry obtained from the simulated annealing procedure was optimized enforcing the convergence criterion that the difference between the total energies obtained in two subsequent steps be less than 0.1 meV. It should be noted that the value of the thermostat mass (Q) and the cooling speed are the most sensitive factors in the simulated annealing process. Performing several simulated annealing runs for selected test systems where the initial structure and the starting temperature were varied, we found the converged final structures were unaffected by these procedural changes. In these tests, the

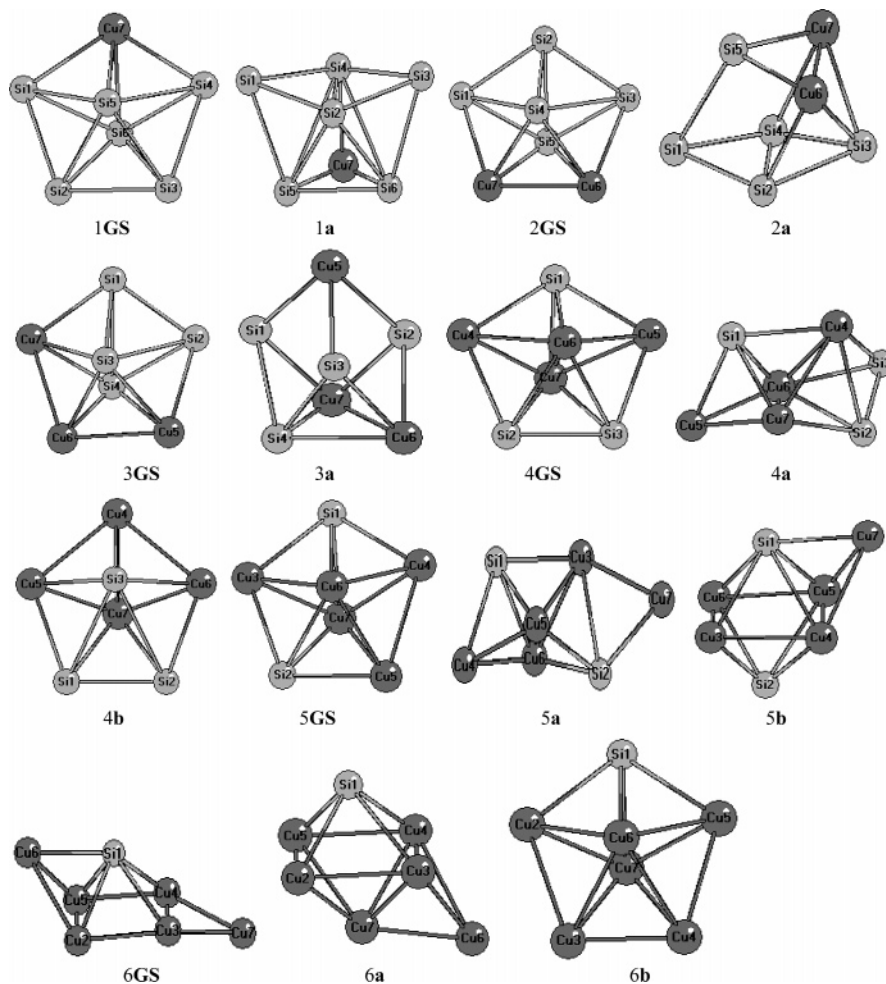


Figure 1. Structure of $\text{Cu}_m\text{Si}_{7-m}$ ($m = 1, 2, \dots, 6$) clusters.

starting temperature ranged from 2000 to 3000 K. However, variation of the value of Q and of the cooling speed resulted in alterations of the final structures. Especially, we observed that a combination of very small Q and fast cooling speed led, for some clusters, to isomers of higher energy. For standard simulated annealing runs, we implemented a cooling speed of $1\text{ }^\circ\text{C}/15\text{ fs}$ and a time step of 3 fs.

To confirm that the structure obtained by the process described above is the ground state, we also carried out geometry optimizations at the B3LYP/6-311+G(d,p) level for the lowest isomers that emerged from the simulated annealing procedure. A detailed discussion of the suitability of the B3LYP method for the treatment of metal–silicon clusters is presented in refs 12 and 29. The agreement of the B3LYP results for various copper–silicon test cases with available experimental values and those obtained by quantum chemical procedures of higher accuracy was generally found to be very satisfactory. The quantum chemical calculations were performed using the Gaussian 03 code.⁴⁹ Three types of geometric arrangements were chosen as input structures, namely, (1) geometries obtained from the above standard simulated annealing and the alternative process that combines a small Q value with a high cooling speed, leading to isomers of higher than the ground state energies, (2) substitutional structures of Si_7 (Cu_7 , Li_7) with metallic atoms at the equatorial sites, (3) structures with face adsorption of the metallic atom on the Si_6^- framework for clusters of composition MeSi_6 . Moreover, we subjected the isomers obtained using the B3LYP/6-311+G(d,p) approach to further optimization by means of the plane wave DFT method as implemented in the

VASP program. The results are presented and discussed in the following section.

Results and Discussion

The structures obtained from our simulated annealing approach and those generated by the quantum chemical computation are plotted in Figures 1 and 2. The isomers of the $\text{Cu}_m\text{Si}_{7-m}$ series labeled as $m\text{GS}$ and ma ($m \leq 6$) are shown in Figure 1, where $m\text{GS}$ refers to the geometry of the ground state (GS) obtained from simulated annealing and ma , mb , ..., indicate the higher energy isomers obtained from the quantum chemical calculations with different initial structures, as mentioned above. The results of $\text{Li}_m\text{Si}_{7-m}$ are shown in Figure 2.

It should be noted that the above GS of each cluster refers to the lowest energy state obtained from optimization by use of the plane wave (PW) DFT method. In each case, the GS is employed as a reference of zero energy. As can be seen from Table 1, the results generated by use of the plane wave and the hybrid density functional (B3LYP) approaches are in good agreement for all of the isomers, except the systems CuSi_6 and Cu_5Si_2 . For all other isomers of the form $\text{Me}_m\text{Si}_{7-m}$ ($\text{Me} = \text{Cu}$, Li), the difference between the geometric parameters obtained by use of the plane wave and the B3LYP method amounts to less than 4%; thus, in the following, the parameters referred to are those obtained by the latter procedure.

1. $\text{Cu}_m\text{Si}_{7-m}$ ($m = 1, 2, \dots, 6$). We comment first on $\text{Cu}_m\text{Si}_{7-m}$ ($m \leq 6$). Cu is one of the most widely used impurities in silicon device fabrication.⁵⁰ As shown by studies of transition-

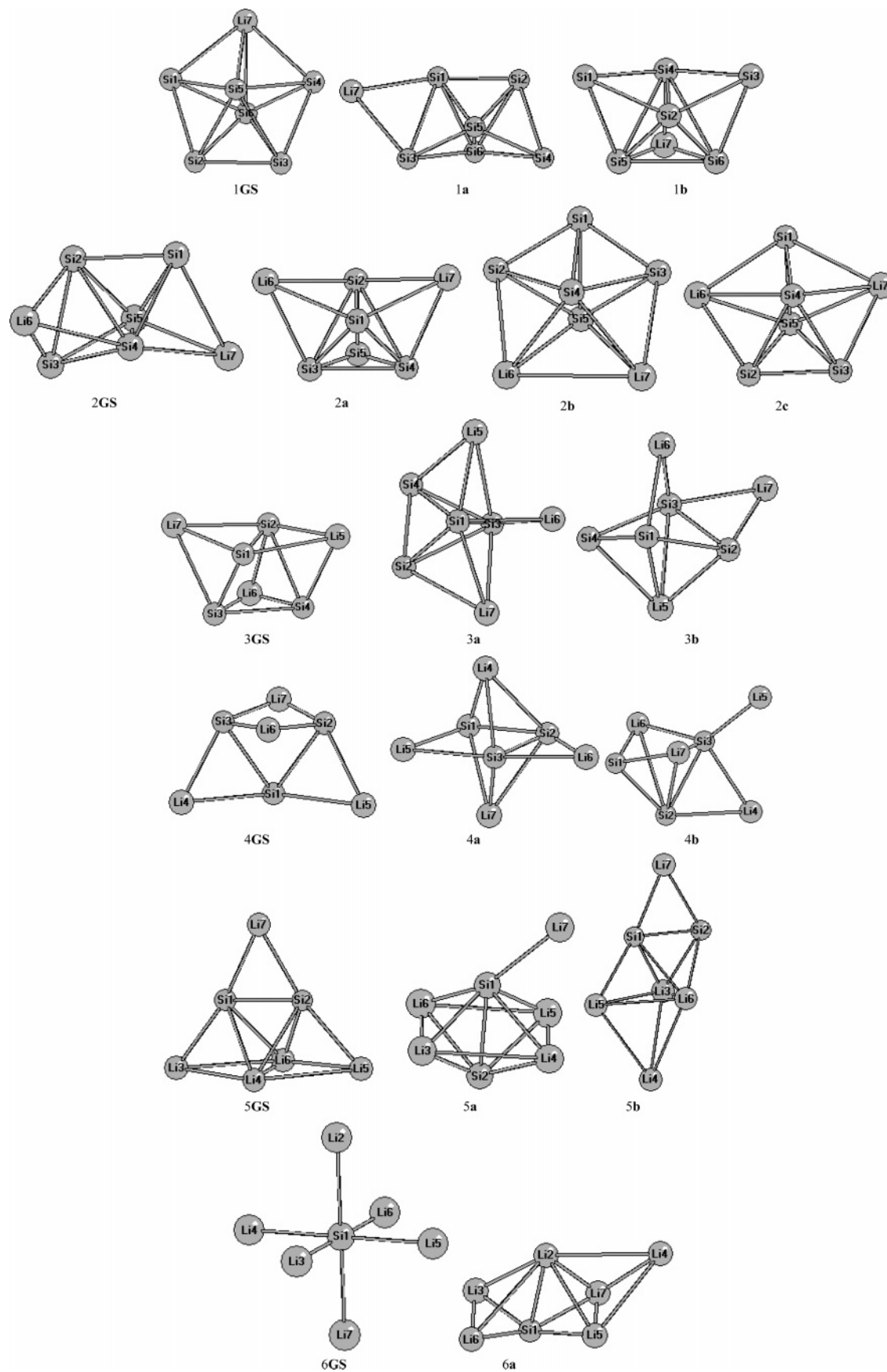


Figure 2. Structure of $\text{Li}_m\text{Si}_{7-m}$ ($m = 1, 2, \dots, 6$) clusters.

metal elements in silicon, they tend to diffuse interstitially and locate at interstitial sites in thermal equilibrium at the diffusion temperature.³⁴ Investigations of copper-doped silicon clusters

demonstrate that Cu in Si_n is likely to occupy a substitutional position derived from the most stable geometry of Si_{n+1} by replacing a Si atom by Cu. The global minima of small Si_n

TABLE 1: Relative Energies and Energy Gaps for the Considered Clusters with Different Isomers

cluster	isomer	relative energy (eV)		energy gap (eV)	
		PW DFT	B3LYP	PW DFT	B3LYP
Si ₇	0GS	0.0	0.0	2.097	3.162
CuSi ₆	1GS	0.0	0.00		
	1a	0.018	−0.078		
Cu ₂ Si ₅	2GS	0.0	0.0	1.827	3.054
	2a	0.070	0.072		
Cu ₃ Si ₄	3GS	0.0	0.0		
	3a	0.073	0.120		
Cu ₄ Si ₃	4GS	0.0	0.0	1.002	2.179
	4a	0.034	0.005		
	4b	0.163	0.104		
Cu ₅ Si ₂	5GS	0.00	0.0		
	5a	0.071	−0.042		
	5b	0.184	0.140		
Cu ₆ Si	6GS	0.0	0.0	1.725	2.602
	6a	0.217	0.242	0.893	1.890
	6b	0.470	0.627	0.409	1.450
LiSi ₆	1GS	0.0	0		
	1a	0.264	0.199		
Li ₂ Si ₅	2GS	0	0	2.103	3.188
	2a	0.016	0.025		
	2b	0.201	0.230		
	2c	0.560	0.494		
Li ₃ Si ₄	3GS	0	0		
	3a	0.374	0.365		
	3b	0.493	0.380		
Li ₄ Si ₃	4GS	0	0	0.915	1.910
	4a	0.004	0.008		
	4b	0.341	0.311		
Li ₅ Si ₂	5GS	0	0		
	5a	0.149	0.107		
	5b	0.157	0.092		
	5c	0.283	0.250		
Li ₆ Si	6GS	0	0	1.025	1.530
	6a	0.350	0.357	0.944	1.679

clusters have been identified by extensive collaborative efforts of theory and spectroscopic measurement.¹¹

The ground state of Si₇ ($m = 0$) is a pentagonal bipyramid (D_{5h}).^{10–12} The geometric parameters of Si₇ are much closer to anionic Si₆[−] than to the neutral Si₆ cluster.¹² Two competitive geometries have been identified for the CuSi₆ ($m = 1$) cluster. The lowest isomer (**1GS**) corresponds to a substitutional structure with Cu occupying an equatorial site. It is near-degenerate with an adsorption site isomer where Cu attaches to a face of the Si₆ frame. From DFT–plane wave calculation, these two alternatives are separated from each other by a small energy difference of 0.018 eV. It should be noted that the approach yields the same order of stabilities for the two structures.¹² The B3LYP/6-311+G(d,p) assessment favors the adsorption site (**1a**) over the substitutional site (**1GS**) by a still small but distinct energy difference of 0.078 eV. Both methods, however, predict the stabilities of the two compared structures to be almost equal.

For $m = 2$, the equilibrium structure (**2GS**) involves two Cu atoms substituting for two Si atoms of the Si₇ cluster at equatorial sites. The five Si atoms arrange in a somewhat distorted D_{3h} structure, and the two Cu atoms form a dimer with an internuclear distance of 2.605 Å. This value may be compared with the bond lengths of Cu₂ (2.278 Å) and Cu₂⁺ (2.449 Å). Thus, the bond distance of the Cu₂ subunit in Cu₂Si₅ is distinctly closer to that of the Cu₂ cation than that of the neutral molecule. This observation is in keeping with the result of natural population analysis,⁵¹ which implies that each Cu atom of Cu₂–Si₅ transfers 0.45*e* to the Si subsystem, as indicated in Table 2. On the other hand, an isomer with two Cu atoms replacing two

TABLE 2: Natural Charge for All Atoms in Selected Isomers by B3LYP/6-311+G(d,p) Analysis^a

cluster	isomer	1	2	3	4	5	6	7
CuSi ₆	1a	0.12	−0.25	0.12	−0.31	−0.10	−0.10	0.52
Cu ₂ Si ₅	2GS	−0.03	−0.23	−0.03	−0.29	−0.32	0.45	0.45
Cu ₃ Si ₄	3GS	−0.24	−0.24	−0.40	−0.40	0.45	0.39	0.45
Cu ₄ Si ₃	4GS	−1.02	−0.44	−0.44	0.47	0.47	0.48	0.48
Cu ₅ Si ₂	5a	−0.84	−0.83	0.38	0.30	0.37	0.37	0.25
Cu ₆ Si	6GS	−1.25	0.27	0.34	0.34	0.27	0.27	−0.24
LiSi ₆	1GS	−0.10	0.05	0.06	−0.10	−0.38	−0.38	<i>0.85</i>
Li ₂ Si ₅	2GS	−0.15	−0.37	−0.15	−0.68	−0.37	<i>0.86</i>	<i>0.86</i>
Li ₃ Si ₄	3GS	−0.53	−0.84	−0.56	−0.53	<i>0.84</i>	<i>0.81</i>	<i>0.81</i>
Li ₄ Si ₃	4GS	−0.83	−1.27	−1.27	<i>0.85</i>	<i>0.85</i>	<i>0.83</i>	<i>0.85</i>
Li ₅ Si ₂	5GS	−1.47	−1.47	<i>0.55</i>	<i>0.49</i>	<i>0.55</i>	<i>0.49</i>	<i>0.88</i>
Li ₆ Si	6GS	−3.60	<i>0.60</i>	<i>0.60</i>	<i>0.60</i>	<i>0.60</i>	<i>0.60</i>	<i>0.60</i>

^a Within the charge data, bold text refers to Cu atoms and italic text refers to Li atoms.

Si atoms at the apical sites of Si₇ turns out to be higher in energy by 1.98 eV than **2GS**, while that with two Cu atoms substituting for two equatorial Si atoms at separated sites is found to be unstable. The isomer of second to lowest stability (**2a**), being higher in energy than **2GS** only by 0.070 eV, is derived from the structure **1a** of CuSi₆ with two Cu atoms at positions 1 and 3 (Figure 1). The architecture of this unit may be described as a Si₄ bent rhombus structure combined with two bonding Cu atoms and the remaining Si atom interacting with both the Si₄ and Cu₂ subsystems.

The ground state of Cu₃Si₄ (**3GS**) is characterized by three Cu atoms substituting for three connected equatorial Si atoms. An initial substitutional structure with three disconnected Cu atoms at the equatorial sites of Si₇ relaxes to **3a**, which is 0.073 eV higher in energy than **3GS**. As the **1a** variant of CuSi₆ is prepared with three Cu atoms at positions 1, 3, and 7 (see Figure 1), relaxation to **3a** is observed as well.

The ground state of Cu₄Si₃ (**4GS**) exhibits a deformed pentagonal shape, resembling the Si₇ species. The three Si atoms locate at the equatorial sites, with two connected Si atoms and one disconnected Si atom. As demonstrated by natural population analysis,¹² the apical Si atoms of Si₇ accept electrons from the equatorial sites. This leads to the expectation that the two apical sites of the Cu₄Si₃ structure based on D_{5h} symmetry should be occupied by Si atoms. This structure, however, is shown to be unstable by B3LYP/6-311+(d,p) analysis. The Cu₄–Si₃ ground state geometry may be understood as originating from the Cu₄ ground state which stabilizes as a bent rhombus. In Cu₄Si₃, the three Si atoms are adsorbed on different sides of this rhombus. An isomer (**4a**) with one Si atom adsorbed on the face of a Si₆-like Cu₄Si₂ framework is found to be 0.034 eV higher in energy than **4GS**. The isomer (**4b**) with one Si atom replacing Cu at an apical position and the other Si atoms occupying equatorial sites as defined by the Cu₇ matrix is 0.163 eV higher in energy than **4GS**. It should be noted that the bent Cu₄ rhombus is present as a structural motif also in the isomer **4a**.

Optimization employing the DFT–plane wave method shows that a structure derived from the D_{5h} prototype (**5GS**) defines the lowest energy state of Cu₅Si₂. DFT analysis at the B3LYP/6-311+G(d,p) level, in contrast, identifies a side-adsorbed isomer (**5a**) with one Cu atom attached to a Si₆[−]-like framework consisting of the four remaining Cu atoms and two Si atoms as being lower in energy than **5GS** by 0.042 eV. Both **5GS** and **5a** can be considered as one Cu atom adsorbed on a Si₆[−]-like substructure, where four Cu atoms form a bent Cu₄ rhombus and two Si atoms locate above and below this rhombus. While simulated annealing at the standard settings employed in this

work produces the **5GS** unit, the alternative choice of parameters mentioned above, involving a small Nosé mass and fast cooling, yields **5a**. The energy difference between these two alternatives is small, amounting to 0.078 eV as the DFT-plane wave method is used and to nearly one-half of this margin in case of the B3LYP treatment. A further isomer (**5b**) is found by DFT-plane wave calculation to be 0.184 eV higher in equilibrium energy than **5GS**. In this case, four Cu atoms form a square and two Si atoms adsorb on the top and bottom of it. A bipyramid structure (D_{4h}) results, to which the remaining Cu atom attaches by face adsorption.

The equilibrium structure of Cu_6Si (**6GS**) deviates from the D_{5h} scheme. Four Cu atoms form the corners of a slightly distorted square. The Si atom is located above the center of this arrangement. Among the residual Cu atoms, one is adsorbed to a SiCu_2 face and the other Cu atom bonds with a Cu_2 subgroup at the opposite side of the Cu_4 motif. This shape might be understood as resulting from the interaction between the pure D_{3h} Cu_6 cluster in its planar equilibrium geometry²² with an adsorbed single Si atom. The isomer **6a** is a structure with five Cu atoms and one Si atom forming a D_{4h} geometry with Si located at the top of the square defined by four Cu atoms. The remaining Cu occupies an adsorption site, interacting with a Cu_3 subgroup. Its energy is 0.217 eV higher than that of **6GS**. Both **6GS** and **6a** may be viewed as two Cu atoms adsorbed on a pyramid framework constructed by a Cu_4 square with Si top adsorption. The substitutional structure of Cu_7 with Si at an equatorial site (**6b**) is less stable than **6GS** by 0.470 eV, and that with Si at an apical site proves to be unstable.

Summarizing the observations made with respect to the preferred structures of the $\text{Cu}_m\text{Si}_{7-m}$ series, we find a strong persistence of the pentagonal motif given by the equilibrium structures of the two homogeneous clusters Si_7 and Cu_7 . This is plausible in light of earlier work on CuSi_n ($n \leq 6$),^{12,33} where it has been shown that Cu as an impurity in a Si_n cluster tends to occupy a substitutional site of Si_{n+1} and correspondingly interacts with its Si neighbors by forming covalent bonds with ionic admixtures. This statement, however, cannot be reversed, since, from the present work, the geometries of CuSi_6 and SiCu_6 turn out to differ substantially. This difference appears to be associated with the deviating equilibrium shapes of the pure clusters Si_6 and Cu_6 , with the former being three-dimensional and the latter being planar. Our investigation suggests that $m = 6$ is the smallest number of Cu constituents in $\text{Cu}_m\text{Si}_{7-m}$ for which the Cu_m subsystem exerts a defining influence on the geometry of the mixed cluster. The ground states of both Cu_4Si_3 and Cu_5Si_2 , as well as their low-lying isomers, exhibit solvation of the $7 - m$ Si atoms in the Cu_m subunit. These atoms do not form a connected subsystem, since at least one of them bonds to Cu atoms only. The structure (**3a**) presents an example for the analogous phenomenon of Cu_m solvation in the Si_{7-m} subunit. This feature demonstrates a certain degree of miscibility of the two elements blended together in $\text{Cu}_m\text{Si}_{7-m}$.

2. $\text{Li}_m\text{Si}_{7-m}$ ($m = 1, 2, \dots, 6$). The electronic structure of lithium is $1s^2 2s^1$. The 2s electron transfers easily to silicon. From our calculations, we find that the ground state structures of $\text{Li}_m\text{Si}_{7-m}$ tend to consist of an anionic Si_{7-m} framework surrounded by m Li atoms that act as electron donors. From natural population analysis, an electronic charge of about $0.8e$ transfers from each Li to Si atoms. In what follows, we comment on individual systems.

The ground state of LiSi_6 (**1GS**) is a deformed bipyramid, like the Si_7 matrix. The Li atom adsorbs on the Si_6^- framework at the equatorial site. The isomer (**1a**) with Li adsorbed on a

Si_2 edge of the Si_6^- framework is higher than **1GS** by 0.264 eV. The energy of isomer **1b**, characterized by face adsorption of Li on Si_6^- , exceeds that of **1GS** by 0.2734 eV, while a substitutional geometry based on Si_7 with Li located at the apical site is found to be less stable than **1GS** by 2.009 eV. As a uniting structural feature of all the explored LiSi_6 isomers (**1GS**, **1a**, and **1b**), the six Si atoms tend to arrange in a Si_6^- configuration, to which the Li atom is attached.

The equilibrium structure (**2GS**) of Li_2Si_5 corresponds to the adsorption of two Li atoms on two different faces of the trigonal bipyramid (D_{3h}) formed by five Si atoms. This Si_5 framework turns out to be more closely related to dianionic Si_5^{2-} than to neutral Si_5 . To be specific, the $1\text{Si}-2\text{Si}$ and $2\text{Si}-4\text{Si}$ bond lengths and the $1\text{Si}-2\text{Si}-3\text{Si}$ angle of Li_2Si_5 are 2.483 Å, 2.411 Å, and 105.580° , respectively, which are much closer to the corresponding parameters in Si_5^{2-} (2.400 Å, 2.606 Å, 102.391°) than in neutral Si_5 (2.329 Å, 3.124 Å, 78.489°). Other isomers (**2a** and **2b**) represent face adsorption patterns involving two Li atoms on adjacent sides of Si_5^{2-} . Both are less stable than **2GS**, by 0.016 and 0.201 eV, respectively. Isomer **2a** is obtained by substituting two Li atoms for Si atoms at positions 1 and 3 of **1a** in CuSi_6 . Isomer **2b** arises from substituting two Li atoms for two equatorial atoms of Si_7 . The salient feature of all of these isomers is that they derive from the Si_5^{2-} trigonal bipyramid, with both Li atoms selecting adsorption sites. Applying natural population analysis (Table 2), we find an overall transfer of about $1.72e$ from the two Li atoms to Si_5 . As a structural peculiarity of Si_5^{2-} in comparison with Si_5 , the axis of the neutral species elongates markedly as two electrons are added to the cluster. A substitutional isomer (**2c**) based on Si_7 , where two Li atoms occupy separated equatorial sites, is determined to be substantially higher in energy than **2GS**, namely, by 0.560 eV.

As one goes to Li_3Si_4 , a face adsorption geometry is identified for the ground state **3GS**. The three Li atoms adsorb on three different sides of Si_4 which adopts tetrahedral geometry. This shape is incompatible with the Si_4 ground state which stabilizes as a planar rhombus (D_{2h}) in the neutral, cationic, and anionic states.¹² The three-dimensional structure of Si_4^{2-} , however, is lower in energy by 0.188 eV than the planar rhombus alternative, as determined by optimization at the B3LYP/6-311+G(d,p) level. Natural population analysis shows that the three Li atoms transfer about $2.46e$ to Si_4 . Thus, the case of Li_3Si_4 demonstrates once more that the Li components in the Si-Li composites considered here act as electron donors and, further, that electron transfer proceeding from the metal subsystem sensitively determines the geometry adopted by the semiconductor subsystem. A further optimization was carried out on the basis of a substantially different initial geometry. More specifically, the CuSi_6 structure (**1a**) was used as a pattern, with Li atoms located at sites 1, 3, and 7 and Si atoms at the remaining sites. This configuration was found to relax to **3GS**. The isomer (**3a**) obtained from an initial D_{5h} based structure where the three Li atoms are placed on connected equatorial positions is 0.374 eV higher in energy than **3GS**. The isomer (**3b**) involves adsorption of the three Li atoms on a bent Si_4 rhombus. This alternative, being less stable than **3GS** by 0.493 eV, is not preferred.

The ground state geometry of Li_4Si_3 (**4GS**) differs strongly from that of Cu_4Si_3 . The three Si atoms form an isosceles elongated Si_3 triangle; a Li_2 subunit bridges between the two Si atoms separated by the smallest distance within this Si_3 motif, and two Li atoms are symmetrically edge adsorbed at the two longer sides of Si_3 . This isosceles elongated Si_3 triangle turns out to be more closely related to trianionic Si_3^{3-} than to neutral

Si₃. To be specific, the 1Si–2Si (1Si–3Si) bond length in Li₄Si₃ is 2.363 Å, which is about 0.025 Å shorter than the corresponding parameter in Si₃³⁻. Likewise, the distance between 2Si and 3Si of Li₄Si₃ is 2.715 Å, which is about 0.364 Å longer than the corresponding parameter in Si₃³⁻. By comparing the relevant charge density distributions, we find the effective charges on the atoms 2Si and 3Si in Li₄Si₃ to be higher by 0.2e than those on their counterpart atoms in Si₃³⁻. The interelectronic repulsion between 2Si and 3Si in Li₄Si₃ elongates the distance between them over that in Si₃³⁻. The ground state has also been attained by employing an initial *D*_{5h} based structure with three Si atoms occupying one equatorial and two apical sites. No similarity is found between the geometry of the Li₄ subsystem of Li₄Si₃ and that of the free Li₄ cluster which has been shown to be planar.^{18,20} The isomer (4a) is obtained from an initial *D*_{5h} based structure with two Si atoms occupying connected equatorial sites and the other Si atom locating at a separate equatorial site, analogous to 1a of CuSi₆ with three Si atoms occupying sites 4, 5, and 6. This structure results in being near-degenerate with 4GS, as both geometries are separated by only 0.004 eV. An isomer (4b) with one Li atom side-adsorbed on a Si₆-like framework formed by Li₃Si₃ exceeds 4GS by 0.341 eV. This framework consists of two Li atoms adsorbed on the top and bottom of the Si₃ plane and the additional Li atom on one of the longer sides of Si₃.

The equilibrium structure of Li₅Si₂ (5GS) possesses a high degree of symmetry. Four of the five Li atoms form a planar rhombus located below a Si dimer, above which the remaining Li atom adsorbs. A slightly different isomer (5b) with the four Li atoms arranged in a diamond structure is by 0.157 eV higher than the 5GS energy. The isomer (5a) with four Li atoms assembled to form a square with one Si atom adsorbed above and the other below the plane defined by this substructure, and the residual Li atom face adsorbed is less stable by 0.149 eV than 5GS.

Turning to Li₆Si (6GS), we find six octahedrally arranged Li atoms surrounding the central Si atom. The 6GS geometry is reproduced by B3LYP/6-311+G(d,p) optimization, where a *D*_{5h} based structure defines the initial geometry. The energy of a further isomer (6a) which derives from the CuSi₆ (1a) prototype is 0.350 eV above that of 6GS.

On the basis of these observations, the members of the Li_{*m*}Si_{7-*m*} group stabilize in characteristically different equilibrium structures than their counterparts of the Cu_{*m*}Si_{7-*m*} series. While substitutional sites are selected by Cu as metal impurity, Li favors adsorption sites, related to different interaction modes of Cu and Li with the Si_{7-*m*} subsystem, namely, the formation of covalent bonds in the former case and stabilization through electron transfer in the latter case. This is in keeping with the observation that the natural charge on Li_{*m*} is substantially higher than that on Cu_{*m*} for all *m* considered. More specifically, Li₂-Si₅ and Li₃-Si₄ can be unambiguously described as Si_{7-*m*} dianions in contact with *m* Li adsorbate atoms, while Li₄Si₃ is more properly understood as involving a somewhat distorted Si₃³⁻ subunit. For *m* > 4, novel structures are found as the resulting Li_{*m*}Si_{7-*m*} equilibrium geometries appear to be dictated neither by the Li_{*m*} nor by the Si_{7-*m*} subsystem.

3. Energy Gaps. It is interesting to examine if the expected narrowing trend of the energy gap as one goes from the purely semiconducting Si₇ system to the purely metallic clusters Li₇ and Cu₇ can be confirmed for the systems investigated in this work. The results emerging from our plane wave basis and B3LYP/6-311+G(d,p) calculations are listed in Table 1. Only the closed-shell clusters are included, that is, Me_{*m*}Si_{7-*m*} with *m*

= 0, 2, 4, 6. Consistently, the energy gaps obtained by the DFT plane wave method are smaller than those determined by use of the hybrid quantum chemical technique by about 1.1 eV. The energy gap 2.097 eV of Si₇ is the same as that indicated in ref 7. A slight reduction of the energy gaps is observed as two metal atoms replace two Si atoms. This moderate change is followed by a drastic decrease as the metal atom count is incremented from two to four. As we proceed to larger complexes, however, the energy gap is found to increase from 1.002 eV in Cu₄Si₃ to 1.725 eV in Cu₆Si. It is worthwhile noting that this conspicuous deviation from the trend suggested by the complexes with fewer Cu atoms correlates with geometry. Thus, the ground state structure of Cu₆Si differs strongly from those of Si₇, Cu₂Si₅, and Cu₄Si₃ which are all variations of the pentagonal pattern defined by the “limiting clusters” Si₇ and Cu₇. The corresponding Cu₆Si isomer (6b) exhibits an energy gap of 0.409 eV which is drastically reduced as compared to that of Cu₄Si₃, namely, by about 0.6 eV. Therefore, by the criterion of energy gap size, the sequence of Cu_{*m*}Si_{7-*m*} isomers with *D*_{5h} based geometries displays the anticipated trend of increasing metallicity with the number *m* of metal atoms contained in the cluster. Within the series of the maximally stable Cu_{*m*}Si_{7-*m*} systems, the unit Cu₆Si presents an exception from this rule.

A similar, although more homogeneous, picture is presented by the Li_{*m*}Si_{7-*m*} series where an energy gap reduction from *m* = 0 to *m* = 4 is contrasted by a slight increase as one goes from *m* = 4 to *m* = 6. This observation is based on the DFT plane wave results, while the B3LYP/6-311+G(d,p) data predict a consistently decreasing trend. Despite the obvious preponderance of the metal atom component in Li₆Si and its peculiar geometry, involving a Si atom octahedrally surrounded by a metal atom shell, both the geometric parameters and the natural charges on the atomic centers of this cluster suggest that it cannot be characterized as metallic. The distance between adjacent Li atoms of *d*(Li–Li) = 3.4 Å, which is markedly elongated by the standard of bond lengths found typically in small Li_{*m*} clusters (*m* ≤ 6),¹⁸ diminishes the interaction between these ligands. Instead, the natural charges listed in Table 2 document a substantial amount of electron transfer from each metal atom to the Si center, giving rise to a complex of pronounced polarity. In view of these features, an energy gap narrowing as one goes from Li₄Si₃ to Li₆Si is not a cogent conclusion.

Summary

The ground state geometries and associated energetic properties of the cluster series Me_{*m*}Si_{7-*m*} (Me = Cu and Li, *m* ≤ 6) were identified by simulated annealing computations, with the use of a global search algorithm being necessitated by the large number of possible atomic permutations for Me_{*m*}Si_{7-*m*} with 1 < *m* < 6. Equilibrium geometries are obtained by the use of a DFT–plane wave formalism in conjunction with the Nosé thermostat scheme. Good agreement is found between the DFT–plane wave basis method and the hybrid quantum chemical method B3LYP at the 6-311+G(d,p) level, except for the cases of CuSi₆ and Cu₅Si₂ where the *D*_{5h} based shapes yielded by the former approach deviate from the geometries resulting from the latter. Within an accuracy of 0.1 eV, however, the order of stabilities among the ground state systems and low-lying isomers as predicted by the two methods agree in all cases considered.

Focusing on the general trends of the ground state equilibrium geometries of Me_{*m*}Si_{7-*m*} (Me = Li and Cu, *m* ≤ 6), one observes that Cu_{*m*}Si_{7-*m*} tends to stabilize in *D*_{5h} based substitutional

geometries, while $\text{Li}_m\text{Si}_{7-m}$ prefers adsorption geometries, involving m Li atoms attached to a Si_{7-m}^{2-} (or Si_{7-m}^{3-}) framework whose architecture is determining for the shape of the cluster as a whole. For $\text{Cu}_m\text{Si}_{7-m}$, an exception from the prevailing pentagonal pattern is given by the system Cu_6Si where the Si atom is adsorbed to a deformed Cu_6 substructure. In contrast, none of the Li_m subsystems resulting from $\text{Li}_m\text{Si}_{7-m}$ optimization bear resemblance to the geometries of any free Li_m clusters. The observed preference of the pentagonal prototype as the structure of $\text{Cu}_m\text{Si}_{7-m}$ clusters suggests a certain extent of interchangeability of Cu and Si constituents in these systems. This trend is further substantiated by the ground state configurations of the species with $m = 2, 3$ where fragmentation of Si_{7-m} is obtained.

The energy gaps of $\text{Me}_m\text{Si}_{7-m}$ ($\text{Me} = \text{Cu}$ and Li , $m \leq 6$) display a narrowing trend with the number of metal constituents, reflecting the increase of cluster metallicity. The species with $m = 6$, however, do not conform with this general tendency. This exceptional behavior appears correlated with the geometric characteristics of the two systems. While Cu_6Si drastically deviates from the D_{5h} based motif that dominates the $\text{Cu}_m\text{Si}_{7-m}$ series, Li_6Si displays octahedral coordination, giving rise to substantial polarity between the Si core and the Li_6 ligand shell.

It will be interesting to extend the present study into the region of mixed metal–semiconductor clusters of intermediate size, with $10 \leq m \leq 50$. Besides its fundamental relevance for the understanding of atomic clusters, such an investigation could contribute to answering the topical question of the degree to which various metal elements can be solvated in finite semiconductor structures.

Acknowledgment. We thank Dr. Sudha Srinivas for helpful and stimulating discussions. This work is supported by the National Science Foundation through the grants HRD-9805465, NSFESP-0132618, and DMR-0304036, by the National Institute of Health through the grant S06-GM008047, and by the Army High Performance Computing Research Center under the auspices of Department of the Army, Army Research Laboratory, under Cooperative Agreement No. DAAD 19-01-2-0014.

References and Notes

- Baletto, F.; Ferrando, R. *Rev. Mod. Phys.* **2005**, *77*, 1.
- Henry, C. R. *Surf. Sci. Rep.* **1998**, *31*, 231.
- Alivisatos, A. P. *Sci. Am.* **2001**, *285*, 66.
- Alivisatos, A. P.; Johnsson, K. P.; Peng, X. G.; Wilson, T. E.; Loweth, C. J.; Bruchez, M. P.; Schultz, P. G. *Nature (London)* **1996**, *382*, 609.
- Bloomfield, L. A.; Freeman, R. R.; Brown, W. L. *Phys. Rev. Lett.* **1985**, *54*, 2246.
- Martin, T. P.; Schaber, H. J. *Chem. Phys.* **1985**, *83*, 855.
- Lu, Z. Y.; Wang, C. Z.; Ho, K. M. *Phys. Rev. B* **2000**, *61*, 2329.
- Rata, I.; Shvartsburg, A. A.; Horoi, M.; Frauenheim, Th.; Siu, K. W. M.; Jackson, K. A. *Phys. Rev. Lett.* **2000**, *85*, 546.
- Sieck, A.; Porezag, D.; Frauenheim, Th.; Peterson, M. R.; Jackson, K. A. *Phys. Rev. A* **1997**, *56*, 4890.
- Raghavachari, K.; Rohlfing, C. M. *J. Chem. Phys.* **1991**, *94*, 3670; **1988**, *89*, 2219.
- Shvartsburg, A. A.; Liu, B.; Jarrold, M. F.; Ho, K. M. *J. Chem. Phys.* **2000**, *112*, 4517.
- Xiao, C.; Hagelberg, F.; Lester, W. A., Jr. *Phys. Rev. B* **2002**, *66*, 075425.
- Jackson, K. A.; Horoi, M.; Chaudhuri, I.; Frauenheim, Th.; Shvartsburg, A. A. *Phys. Rev. Lett.* **2004**, *93*, 013401.
- Prendergast, D.; Grossman, J. C.; Williamson, A. J.; Fattebert, J.-L.; Galli, G. *J. Am. Chem. Soc.* **2004**, *126*, 13827.
- Marim, L. R.; Lemes, M. R.; Dal Pino, A., Jr. *Phys. Rev. A* **2003**, *67*, 033203.
- Knight, W. D.; Clemenger, K.; de Heer, W. A.; Saunders, W. A.; Chou, M. Y.; Cohen, M. L. *Phys. Rev. Lett.* **1984**, *52*, 2141.
- Bonacić-Koutecký, V.; Fantucci, P.; Koutecký, J. *Phys. Rev. B* **1988**, *37*, 4369.
- Boustani, I.; Pewestorf, W.; Fantucci, P.; Bonacić-Koutecký, V.; Koutecký, J. *Phys. Rev. B* **1987**, *35*, 9437.
- Ishikawa, Y.; Sugita, Y.; Nishikawa, T.; Okamoto, Y. *Phys. Lett. A* **2001**, *333*, 199.
- Srinivas, S.; Jellinek, J. *Phys. Status Solidi* **2000**, *217*, 311.
- Alonso, J. A. *Chem. Rev.* **2000**, *100*, 637.
- Jug, K.; Zimmermann, B.; Calaminici, P.; Köster, A. M. *J. Chem. Phys.* **2002**, *116*, 4497.
- Fujima, N.; Yamaguchi, T. *J. Phys. Soc. Jpn.* **1989**, *58*, 1334.
- Beck, S. M. *J. Chem. Phys.* **1989**, *90*, 6306.
- Hiura, H.; Miyazaki, T.; Kanayama, T. *Phys. Rev. Lett.* **2001**, *86*, 1733.
- Han, J. G.; Shi, Y. Y. *Chem. Phys.* **2001**, *266*, 33.
- Han, J. G.; Hagelberg, F. *Chem. Phys.* **2001**, *263*, 55.
- Xiao, C.; Hagelberg, F. *THEOCHEM* **2000**, *529*, 241.
- Ovcharenko, I. V.; Lester, W. A., Jr.; Xiao, C.; Hagelberg, F. *J. Chem. Phys.* **2001**, *114*, 9028.
- Kumar, V.; Kawazoe, Y. *Phys. Rev. Lett.* **2001**, *87*, 045503.
- Scherer, J. J.; Pau, J. B.; Collier, C. P.; Saykally, R. J. *J. Chem. Phys.* **1995**, *102*, 5190; **1995**, *103*, 113.
- Scherer, J. J.; Pau, J. B.; Collier, C. P.; O'Keefe, A.; Saykally, R. J. *J. Chem. Phys.* **1995**, *103*, 9187.
- Xiao, C.; Abraham, A.; Quinn, Q.; Hagelberg, F.; Lester, W. A., Jr. *J. Phys. Chem. A* **2002**, *106*, 11380.
- Weber, E. R. *Appl. Phys. A* **1983**, *30*, 1.
- Kresse, G.; Hafner, J. *Phys. Rev. B* **1993**, *47*, 558; **1994**, *49*, 14251.
- Kresse, G.; Furthmüller, J. *Comput. Mater. Sci.* **1996**, *6*, 15.
- Mermin, N. D. *Phys. Rev.* **1965**, *140*, A1141.
- Perdew, J. P.; Zunger, A. *Phys. Rev. B* **1981**, *23*, 5048.
- Kohn, W.; Sham, L. J. *Phys. Rev.* **1965**, *140*, A1133.
- Wood, D. M.; Zunger, A. *J. Phys. A* **1985**, *18*, 1343.
- Pulay, P. *Phys. Lett.* **1980**, *73*, 393.
- Blöchl, P. E. *Phys. Rev. B* **1994**, *50*, 17953.
- Perdew, J. P.; Wang, Y. *Phys. Rev. B* **1992**, *45*, 13244.
- Perdew, J. P.; Burke, K.; Ernzerhof, M. *Phys. Rev. Lett.* **1996**, *77*, 3865.
- Nosé, S. *J. Chem. Phys.* **1984**, *81*, 511.
- Bylander, D. M.; Kleinman, L. *Phys. Rev. B* **1992**, *46*, 13756.
- Gear, C. W. *Numerical Initial Value Problem in Ordinary Differential Equations*; Prentice Hall: Englewood Cliffs, NJ, 1971; Chapters 9 and 10.
- Arnold, A.; Mauser, N.; Hafner, J. *J. Phys.: Condens. Matter* **1989**, *1*, 965.
- Frisch, M. J.; Trucks, G. W.; Schlegel, H. B.; Scuseria, G. E.; Robb, M. A.; Cheeseman, J. R.; Montgomery, J. A., Jr.; Vreven, T.; Kudin, K. N.; Burant, J. C.; Millam, J. M.; Iyengar, S. S.; Tomasi, J.; Barone, V.; Mennucci, B.; Cossi, M.; Scalmani, G.; Rega, N.; Petersson, G. A.; Nakatsuji, H.; Hada, M.; Ehara, M.; Toyota, K.; Fukuda, R.; Hasegawa, J.; Ishida, M.; Nakajima, T.; Honda, Y.; Kitao, O.; Nakai, H.; Klene, M.; Li, X.; Knox, J. E.; Hratchian, H. P.; Cross, J. B.; Bakken, V.; Adamo, C.; Jaramillo, J.; Gomperts, R.; Stratmann, R. E.; Yazyev, O.; Austin, A. J.; Cammi, R.; Pomelli, C.; Ochterski, J. W.; Ayala, P. Y.; Morokuma, K.; Voth, G. A.; Salvador, P.; Dannenberg, J. J.; Zakrzewski, V. G.; Dapprich, S.; Daniels, A. D.; Strain, M. C.; Farkas, O.; Malick, D. K.; Rabuck, A. D.; Raghavachari, K.; Foresman, J. B.; Ortiz, J. V.; Cui, Q.; Baboul, A. G.; Clifford, S.; Cioslowski, J.; Stefanov, B. B.; Liu, G.; Liashenko, A.; Piskorz, P.; Komaromi, I.; Martin, R. L.; Fox, D. J.; Keith, T.; Al-Laham, M. A.; Peng, C. Y.; Nanayakkara, A.; Challacombe, M.; Gill, P. M. W.; Johnson, B.; Chen, W.; Wong, M. W.; Gonzalez, C.; Pople, J. A. *Gaussian 03*, revision C.02; Gaussian, Inc.: Wallingford CT, 2004.
- Istratov, A. A.; Weber, E. R. *Appl. Phys. A* **1998**, *66*, 123.
- Foster, J. P.; Weinhold, F. *J. Am. Chem. Soc.* **1980**, *102*, 7211.
- Reed, A. E.; Weinhold, F. *J. Chem. Phys.* **1983**, *78*, 4066.
- Reed, A. E.; Weinstock, R. B.; Weinhold, F. *J. Chem. Phys.* **1985**, *83*, 735.